

Constraining the instantaneous aerosol influence on cloud albedo

Edward Gryspeerdt^{a,b,1}, Johannes Quaas^a, Sylvaine Ferrachat^c, Andrew Gettelman^d, Steven Ghan^e, Ulrike Lohmann^c, Hugh Morrison^d, David Neubauer^c, Daniel G. Partridge^{f,g}, Philip Stier^h, Toshihiko Takemuraⁱ, Hailong Wang^e, Minghui Wang^{j,k,l,e}, and Kai Zhang^e

^aInstitute for Meteorology, Universität Leipzig, Leipzig, Germany; ^bSpace and Atmospheric Physics Group, Imperial College London, London SW7 2AJ, United Kingdom; ^cInstitute for Atmospheric and Climate Science, ETH Zurich, 8092 Zurich, Switzerland; ^dNational Center for Atmospheric Research, Boulder, CO 80305; ^eAtmospheric Sciences and Global Change Division, Pacific Northwest National Laboratory, Richland, WA 99352; ^fDepartment of Environmental Science and Analytical Chemistry, Stockholm University, Stockholm, Sweden; ^gBert Bolin Centre for Climate Research, Stockholm University, Stockholm, Sweden; ^hAtmospheric, Oceanic and Planetary Physics, Department of Physics, University of Oxford, Oxford, OX1 3PU, United Kingdom; ⁱResearch Institute for Applied Mathematics, Kyushu University, Fukuoka 816-8580, Japan; ^jInstitute for Climate and Global Change Research, Nanjing University, 210023 Nanjing, China; ^kSchool of Atmospheric Sciences, Nanjing University, 210023 Nanjing, China; ^lCollaborative Innovation Center of Climate Change, 210023 Nanjing, China

This manuscript was compiled on May 2, 2017

Much of the uncertainty in estimates of the anthropogenic forcing of climate change comes from uncertainties in the instantaneous effect of aerosols on cloud albedo, known as the Twomey effect or the radiative forcing from aerosol-cloud interactions (RFaci) a component of the total or effective radiative forcing (ERFaci). As aerosols serving as cloud condensation nuclei (CCN) can have a strong influence on the cloud droplet number concentration (N_d), previous studies have used the sensitivity of the N_d to aerosol properties as a constraint on the strength of the RFaci. However, recent studies have suggested that relationships between aerosol and cloud properties in the present day climate may not be suitable for determining the sensitivity of the N_d to anthropogenic aerosol perturbations. Using an ensemble of global aerosol-climate models, this study demonstrates how joint histograms between N_d and aerosol properties can account for many of the issues raised by previous studies. It shows that if the anthropogenic contribution to the aerosol is known, the RFaci can be diagnosed to within 20% of its actual value. The accuracy of different aerosol proxies for diagnosing the RFaci is investigated, confirming that using the aerosol optical depth (AOD) significantly underestimates the strength of the aerosol-cloud interactions in satellite data.

Aerosols | Clouds | Radiative Forcing

The radiative forcing due to anthropogenic aerosols is the most uncertain component of the anthropogenic radiative forcing [1], with the interaction between aerosols and clouds generating much of this uncertainty. As cloud droplets form on aerosol particles, changes in the aerosol number concentration can change the cloud droplet number concentration (N_d), generating an instantaneous radiative forcing by increasing the cloud brightness known as the “Twomey effect” [2] or RFaci [1] (referring only to liquid clouds in this work). Together with other changes in cloud properties due to changes in N_d [eg. 3], the RFaci is a component of the ERFaci.

Due to the sparse nature of pre-industrial observations of cloud properties, the influence of aerosols on cloud properties is often inferred from observations of the present-day spatio-temporal variability of aerosol and cloud properties [eg. 4–7]. While much of the variation between aerosol and cloud properties can be attributed to variations of meteorological factors [eg. 8, 9], the sensitivity of N_d to aerosol optical depth (AOD) is thought to be largely independent of these factors. It is therefore often used in observational estimates of the strength of aerosol-cloud interactions [7, 10, 11]. This sensitiv-

ity [5] has been shown to be a useful “emergent constraint” on the strength of the ERFaci in general circulation models [12], providing a method to calculate the change in N_d from the pre-industrial (PI) to the present day (PD), when combined with an estimate of the corresponding anthropogenic change in AOD (such as [13]). Two main assumptions are made in this process, firstly that the AOD is a suitable proxy of the cloud condensation nuclei (CCN) concentration at the cloud base. Second, that the relationships between aerosol and the N_d in the present day (determined by spatio-temporal variability) are indicative of the actual sensitivity of cloud properties to aerosol perturbations.

Recent work has called both of these assumptions into question. Observational [14] and model-based [15] studies have shown a disconnect between AOD and CCN. As the AOD is a column integrated measurement, it does not provide vertical information about the location of the aerosol. It also lacks information about the composition of the particles and is weighted preferentially towards larger particles [4], missing information about smaller aerosol particles that are often emitted from anthropogenic activities [16].

Second, it has been shown that the PD AOD- N_d relationship may not be representative of the true strength of the

Significance Statement

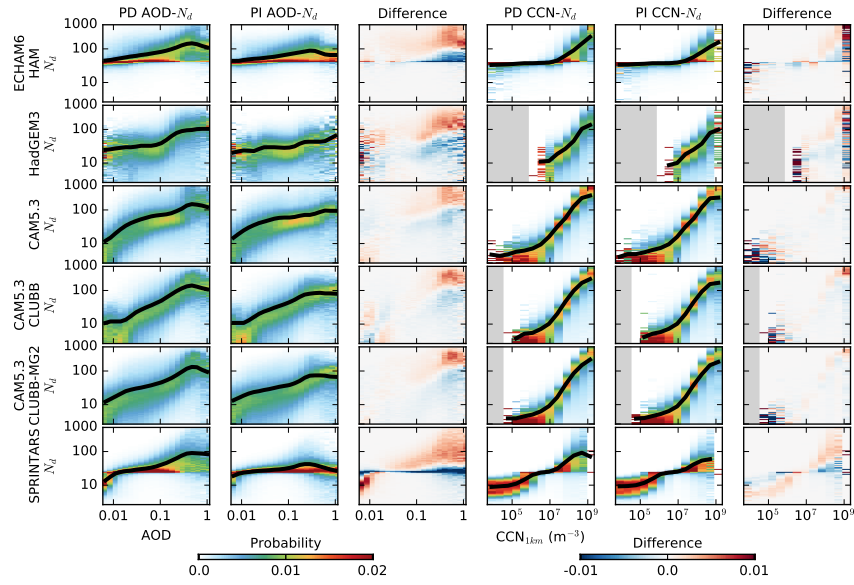
Uncertainties in the strength of aerosol-cloud interactions drive the current uncertainty in the anthropogenic forcing of the climate. Previous studies have highlighted shortcomings in using satellite data for determining the forcing, which underestimate the strength of the aerosol forcing. This work demonstrates that the component of the radiative forcing from aerosol-cloud interactions due to the instantaneous effect on cloud reflectivity (RFaci) can be calculated to within 20%, using only present day observations of the variability of aerosol and cloud properties, provided the anthropogenic component of the aerosol is known. The model results are combined with satellite data to provide an improved observations-based estimate of the RFaci, paving the way for more accurate estimates of the aerosol influence on climate.

EG and JQ wrote the paper, EG performed the analysis, SF, AG, SG, UL, HM, DN, DGR, PS, TT, HW, MW and KZ contributed new reagents/analytic tools.

The authors declare no conflicts of interest.

¹To whom correspondence should be addressed. E-mail: e.gryspeerdt@imperial.ac.uk

125
126
127
128
129
130
131
132
133
134
135
136
137
138
139
140
141
142
143
144
145
146
147
148
149
150
151
152
153
154
155
156
157
158
159
160
161
162
163
164
165
166
167
168
169
170
171
172
173
174
175
176
177
178
179
180
181
182
183
184
185
186



187
188
189
190
191
192
193
194
195
196
197
198
199
200
201
202
203
204
205
206
207
208
209
210
211
212
213
214
215
216
217
218
219
220
221
222
223
224
225
226
227
228
229
230
231
232
233
234
235
236
237
238
239
240
241
242
243
244
245
246
247
248

Fig. 1. Joint histograms between aerosol properties (AOD and CCN_{1km} , respectively, x-axis) and cloud top N_d (y-axis) for each of the GCMs used in this study. The first and second columns show the AOD- N_d joint histograms for the present day and the pre-industrial simulations respectively. The histograms are normalised so each column sums to one, such that the histograms show the probability of observing a specific cloud top N_d , given a certain AOD (or CCN_{1km}). The black line shows the mean N_d at each AOD and grey regions indicate missing data. The third column shows the difference between the present day and the pre-industrial relationships. The second set of three columns are the same as the first three, but use CCN_{1km} at 0.3% supersaturation instead of AOD as the independent variable.

interaction between aerosols and cloud properties due to the differing PI and PD aerosol environments [17]. Additionally, it has been shown [18] that in many global aerosol-climate models, the PD sensitivity of N_d to CCN variations (the slope of the linear regression between N_d and CCN concentrations) is in many cases not representative of the sensitivity of N_d to the anthropogenic perturbation of CCN (the PD-PI change in N_d divided by the corresponding change in CCN evaluated from climate simulations). This suggests that it would be challenging to constrain the magnitude of the RFac using only PD observations of the sensitivity of N_d to aerosol variations.

In this work, new techniques are presented to address these challenges. To account for non-linearity in the aerosol- N_d relationship and the differing PI and PD aerosol environments, normalised joint histograms are used to characterise the relationship [following 11]. A variety of different global aerosol-climate models that contributed to the AeroCom intercomparison [18, 19] are used to investigate the utility of different aerosol proxies for diagnosing the anthropogenic change in cloud-top N_d . Together with joint histograms, this work investigates how accurately the RFac could be diagnosed under ideal conditions, using present day relationships between aerosol and cloud properties.

Results

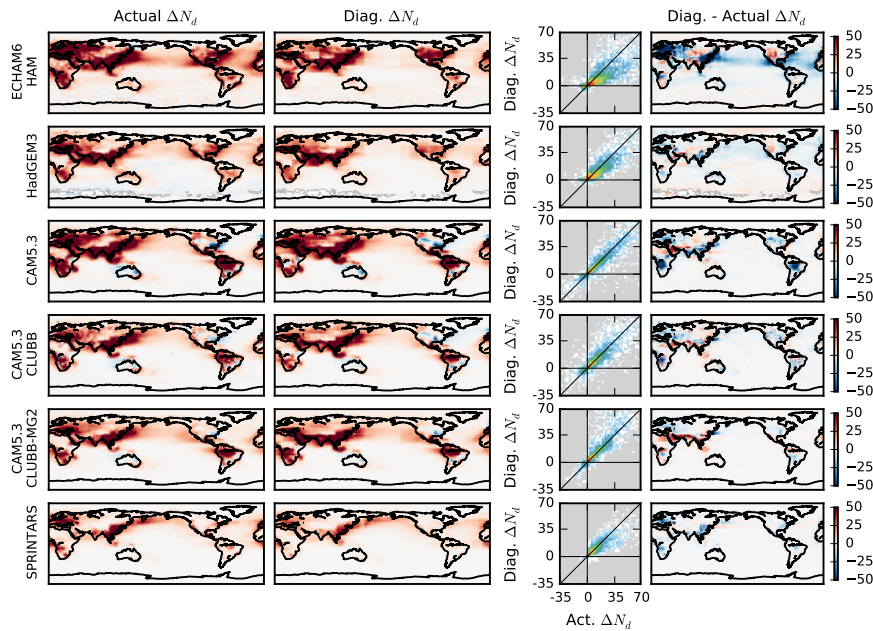
Aerosol- N_d relationships. Two-dimensional (“joint”) histograms of N_d and aerosol properties are used in this work to account for the influence of non-linearities in the relationship [11]. Each column of the joint histogram is normalised so that it sums to one, such that it becomes an array of conditional probabilities. For example, the top left histogram in Fig. 1 shows the probability of finding a specific N_d , given that a certain AOD has been observed.

Joint histograms of cloud top N_d versus an aerosol proxy for a selection of models from the AeroCom intercomparison [18, 19] (gridded to 2.5° by 2.5°) are shown in Fig. 1. While there is a general increase in cloud top N_d with increasing AOD (Fig. 1, first and second columns), the nature of this increase varies significantly amongst the models. Some of the models (the CAM5 variants) show a strong increase in N_d at lower AOD, followed by a saturation at higher AOD, where the N_d only weakly increases with increasing AOD. Others show a weak AOD- N_d relationship at low AOD, followed by a stronger relationship as the AOD increases (ECHAM6-HAM, SPRINTARS). The enforced lower bound to the N_d apparent in some simulations may be responsible for the lower sensitivity of N_d to AOD ($\frac{dN_d}{dln(A)}$) at low AODs in these models [12], although low sensitivities at low AOD have also been observed in satellite data [11].

All of the models show some difference in the AOD- N_d relationship between the PD and the PI (Fig. 1, third column), mostly with higher N_d s for a given AOD in the PD simulation compared to the PI. It is stronger at high AODs, suggesting that this effect is due to the different composition of aerosols in the PD compared to the PI. When the atmosphere is clean (low AOD), the aerosol composition is similar in the PI and the PD simulations. However, high AOD conditions occur mainly in dusty regions in the PI simulation (where the aerosol is a poor CCN), but in the PD simulation, these high AOD conditions are often the result of anthropogenic pollution (which on average is a much better CCN).

The situation is very different when using CCN at 1 km altitude and 0.3% supersaturation (CCN_{1km}) instead of the AOD as the parameter representing the aerosol (Fig. 1, fourth column). The CCN_{1km} - N_d relationships are still mostly non-linear, although there is less variation between the models than for the AOD- N_d joint histograms. Importantly, the PD and

249
250
251
252
253
254
255
256
257
258
259
260
261
262
263
264
265
266
267
268
269
270
271



311
312
313
314
315
316
317
318
319
320
321
322
323
324
325
326
327
328
329
330
331
332
333

272 **Fig. 2.** Using joint histograms of CCN_{1km} vs. N_d from 15° by 15° regions to diagnose ΔN_d (Hist CCN regional). For each model used, the first column shows the
273 annual-mean “actual” ΔN_d (the N_d difference between the PI and PD simulations). The second shows ΔN_d diagnosed using the present day CCN_{1km} - N_d joint histogram
274 and the change in the CCN_{1km} between the PI and PD simulations. The third column shows the relationship between the actual and the diagnosed ΔN_d , whilst the final
275 column shows the absolute difference between the diagnosed and the actual ΔN_d , with red indicating an overestimation in ΔN_d diagnosed from the present day relationships
276 compared to the actual value. The same color scale is used for all maps and all the N_d units are cm^{-3} .

277
278 PI CCN_{1km} - N_d relationships are very similar, showing much
279 smaller differences in the joint histograms than are evident
280 for the AOD- N_d relationship (Fig. 1, sixth column). At lower
281 supersaturations (0.1%) the CCN is weighted towards larger
282 particles and the PD and PI relationships are not as close (Fig.
283 S10). However, the PD global CCN_{1km} - N_d joint histogram is
284 a reasonable indicator of the PI relationship, as long as there
285 is enough data at low CCN concentrations to properly create
286 a joint histogram.

287 It is also clear that the non-linearity of these relationships
288 will influence any calculations made using a linear regression,
289 where the sensitivity would otherwise depend on the prevailing
290 aerosol environment [17]. By normalising the joint histograms
291 by the aerosol occurrence, this dependence is removed and
292 with the appropriate choice of aerosol proxy (such as CCN_{1km}),
293 the PD spatio-temporal variability is a good approximation of
294 the PI variation and thus the actual sensitivity of clouds to
295 aerosol perturbations.

296 **Diagnosing ΔN_d .** Using regional joint histograms (15° by 15°
297 regions), similar to those from Fig. 1, and probability histo-
298 grams for CCN_{1km} from the PI and PD simulations, a pre-
299 diction for the geographic distribution of ΔN_d is constructed
300 in Fig. 2. The “actual” ΔN_d for each model (the difference
301 in N_d between the PD and PI simulations) is shown in the
302 first column of Fig. 2. Both the PI and PD simulations are
303 nudged to the same horizontal winds, such that the “actual”
304 ΔN_d is due to the difference in aerosol emissions. The ΔN_d
305 diagnosed using the PD CCN_{1km} - N_d joint histogram and the
306 PD-PI CCN_{1km} change (Eq. 1) is shown in the second column.

307 There is a good correspondence between the diagnosed and
308 the actual ΔN_d (Fig. 2, third column). The correlation
309 coefficients between the diagnosed and actual ΔN_d are between
310

0.84 and 0.92, explaining between 70% and 85% of the variance
(Fig. 3a). These correlations decrease slightly if a single global
joint histogram is used (Fig. 3a). The difference between
the diagnosed and the actual ΔN_d in the fourth column of
Fig. 2 varies between the models, partially due to remaining
difference between the daily mean CCN_{1km} and the cloud base
 CCN . This appears to be important for the ECHAM6-HAM
simulation over ocean (Fig. 2), where the 1km level is more
often above the cloud tops in stratocumulus regions [20] than
in the other models. Repeating the analysis using the total
column CCN at 0.3% supersaturation (“col CCN ”) improves
the ΔN_d and R $_{Faci}$ diagnosis for ECHAM6-HAM (Fig. 3b,c),
possibly due to the extra information provided about cloud
base CCN . Regime dependent updraughts may also play a role
in controlling the remaining 20% of the variability in ΔN_d
(Fig. 3b). It is possible that there is further variability in
 ΔN_d from PI-PD differences in the parametrised updraughts
(which might be reduced by the nudging procedure) but this is
a small component of the total variability and so is not further
considered in this analysis. These results show that through
the ability of the PD CCN_{1km} - N_d relationship to provide
information on the “actual” CCN_{1km} - N_d relationship, the PD
relationship can be used to provide an accurate estimate of
the ΔN_d due to anthropogenic aerosol perturbations, as long
as that perturbation is known.

Comparison of aerosol proxies. Although ΔN_d can be diag-
nosed through the PD CCN_{1km} - N_d relationship, observations
of CCN_{1km} are sparse in both space and time, necessitating
the use of other aerosol proxies for diagnosing ΔN_d . The
aerosol index (“AI” - AOD multiplied by Angström exponent
[4]) is routinely observed by satellites and provides more in-
formation about aerosol size than the AOD. Although not

334
335
336
337
338
339
340
341
342
343
344
345
346
347
348
349
350
351
352
353
354
355
356
357
358
359
360
361
362
363
364
365
366
367
368
369
370
371
372

373
374
375
376
377
378
379
380
381
382
383
384
385
386
387
388
389
390
391
392
393
394
395
396
397
398
399
400
401
402
403
404
405
406
407
408
409
410
411
412
413
414
415
416
417
418
419
420
421
422
423
424
425
426
427
428
429
430
431
432
433
434

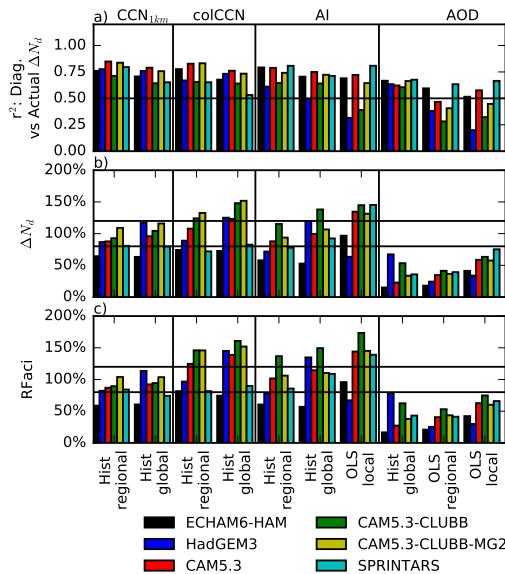


Fig. 3. Comparison of different methods and proxies for calculating ΔN_d . “Hist” indicates the use of a joint histogram while “OLS” the use of an ordinary least-squares regression. a) Shows the determination coefficient between the diagnosed and the actual values of the ΔN_d at a 2.5° by 2.5° resolution globally. b) Shows the relative size of the global mean ΔN_d and c) shows the relative size of the implied global mean RFac, with a percentage less than 100% indicating an underestimate in the estimated RFac. The horizontal bars are at 80% and 120%. The plots summarised in this figure are shown in Figs. S1-9.

currently retrieved by satellites, colCCN provides extra information about the aerosol chemistry. For each of these proxies, the determination coefficient (r^2) between the diagnosed and the actual ΔN_d is shown in Fig. 3a (see Figs. S1-9 for other aerosol proxies). For comparison with earlier work, linear regressions between the N_d and aerosol proxies are also used to characterise the PD aerosol- N_d relationship (“OLS”). The relationships are determined at several different scales: 2.5° by 2.5° degree - “local”; 15° by 15° - “regional” and a single global relationship “global”. The “local” scale is only used with the OLS method, as there is not enough data within each gridbox to generate a full joint histogram.

Using separate regional PD joint histograms between CCN_{1km} and N_d (Fig. 3a, Hist regional) is best able to predict ΔN_d for each of the models investigated here (excluding ECHAM6-HAM). A single global joint CCN_{1km}- N_d histogram (Hist global) results in a slight decrease in the ability to predict ΔN_d . There is again a slight weakening in predictive ability when moving to the colCCN as a proxy for diagnosing ΔN_d . The AI also provides a reasonable parameter for characterising the aerosol, in many cases producing an accurate estimate of ΔN_d (Fig. 3b). Using regional AI- N_d joint histograms for diagnosing ΔN_d gives r^2 values between the diagnosed and the actual ΔN_d (0.61 to 0.81) approaching those of the CCN_{1km}. As the models do not provide the RFac, the relative error in the RFac is estimated by weighting ΔN_d by the observed liquid cloud fraction and cloud albedo susceptibility (Fig. 3c, see methods section for details). In general, the regional joint histograms provide a more accurate diagnosis of RFac, although using a single global histogram results in only a small increase in the error, even though the r^2 value decreases for all

the models (Fig. 3a). The AOD performs worst as a parameter for characterising aerosol in the models when diagnosing ΔN_d and RFac. The local linear regressions have the lowest r^2 values of all the methods and proxies investigated, although the RFac estimate when using AOD is slightly improved compared to the regional linear regression, possibly due to the reduced aerosol type variability for a local regression (Fig. 3c).

From these results, it is clear that estimates of the aerosol forcing that rely on the relationship between AOD and N_d for characterising the strength of aerosol cloud interactions (such as many observational estimates) are likely to underestimate the anthropogenic perturbation of N_d by at least 30% (up to 90%). This would lead to an underestimate in the strength of the radiative forcing from aerosol indirect effects in these studies of at least 20% (up to 90%).

Satellite based estimate. Although using the AOD as an aerosol proxy can lead to an underestimate when diagnosing the aerosol forcing, the AI is almost as good a proxy for the aerosol as the CCN_{1km} when attempting to diagnose ΔN_d and the RFac (Fig. 3c). Given this improved accuracy when compared to using AOD as an aerosol proxy, MODIS AI and N_d data is used to generate both regional joint histograms (Hist AI regional, 15° by 15° regions) and a single global joint histogram (Hist AI global), using 10 years of data (2004-2013). These are then combined with the annual mean MODIS liquid cloud fraction and the cloud susceptibility derived from MODIS and CERES (Eq. 3) to provide an updated estimate of the RFac (Fig. 4).

Using the PI to PD AI changes from each of the models gives a range of RFac estimates for the regional method between -0.18 and -0.58 Wm^{-2} and between -0.29 and -1.01 Wm^{-2} if using a single global AI- N_d joint histogram (Fig. S11). The RFac is generally higher over the ocean due to the higher liquid cloud fraction and cloud susceptibility, despite the smaller oceanic ΔN_d (Fig. 2). Although this is not a large selection of models, the mean value of -0.29 Wm^{-2} for the regional method and -0.49 Wm^{-2} for the global histogram are instructive to compare to the -0.2 Wm^{-2} mean value using a single global AOD- N_d histogram (Fig. 4c), -0.2 Wm^{-2} using local OLS with AOD [7] and -0.4 Wm^{-2} using local OLS and AI [21].

There are some caveats to this estimate. First, the MODIS AI has little quantitative skill over land [22] and in some regions a positive RFac is diagnosed from changes in the N_d (Fig. 4). This has a larger impact on the regional histogram method and may result in a reduction in the strength of the implied aerosol forcing. However, only a small fraction of the forcing comes from continental regions, similar to the findings from [7], so this may not result in a large bias in the global mean RFac. Also, the global histogram method is more likely to overestimate the RFac (Fig. 3c), suggesting that the actual value is between the two estimates, perhaps around -0.4 Wm^{-2} (this only includes changes to cloud albedo and not other rapid cloud adjustments). It is also possible that systematic biases in the MODIS AI or N_d retrieval could further impact this result, although the magnitude and sign of these effects is unclear. It should also be noted that this estimate is strongly dependent on the estimate of the anthropogenic aerosol fraction. As all the AeroCom models in this work use the same emissions database, the diversity in the forcing estimates from the models is unlikely to fully represent the full uncertainty in the radiative forcing from changes in cloud albedo.

497
498
499
500
501
502
503
504
505
506
507
508
509
510
511
512
513
514
515
516
517
518
519
520
521
522
523
524
525
526
527
528
529
530
531
532
533
534
535
536
537
538
539
540
541
542
543
544
545
546
547
548
549
550
551
552
553
554
555
556
557
558

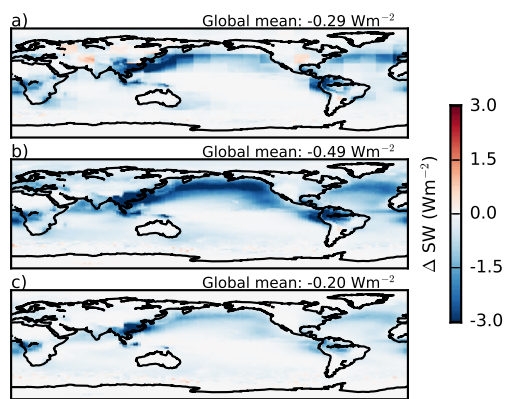


Fig. 4. The mean of the individual model RFac estimates (Fig. S11), using MODIS data to create a) Regional histograms, b) a single global AI- N_d histogram and c) a single global AOD- N_d histogram, combined with model estimates of the anthropogenic AI/AOD contribution.

Discussion

Previous work has shown that the present day CCN- N_d relationship sampled from spatio-temporal variability is not necessarily representative of the “actual” sensitivity of N_d to aerosol changes since pre-industrial times. This is partially due to the large errors in the sensitivity of the N_d to CCN in clean regions, where there is little CCN variation and consequently little N_d variation in the PD climate. However, these regions are usually regions with a small anthropogenic CCN contribution and so make only a small contribution to the global ΔN_d . Although the nudging process might reduce the variability in ΔN_d from variations in the in-cloud updraughts, this work demonstrates that the CCN_{1km} - N_d relationship is representative enough in regions where there is a large ΔN_d to make an accurate prediction of the global ΔN_d and RFac.

It is also interesting to note that the big increases in N_d occur in regions with large changes in CCN (over land, the northern hemisphere) in all the models investigated here (Fig. 2). While these models implement aerosol activation parametrisations that result in a saturation of the N_d at high CCN concentrations, this behaviour is not evident in many of the joint histograms of Fig. 1 for the CCN_{1km} versus the N_d . Although there are other non-linearities in the pathway between CCN changes and a change in top of atmosphere albedo [eg. 11], strong aerosol-cloud interaction effects also occur in regions of stronger aerosol perturbation for the CMIP5 models (albeit less concentrated in the northern hemisphere) [23], supporting the idea that the RFac in remote regions such as the southern ocean does not dominate the total RFac.

Finally, the results of this work demonstrate the importance of including aerosol size information when making estimates of the aerosol impact on cloud properties. Previous work has shown that the AI correlates better than the AOD with the cloud base CCN [15]. This work shows that it also offers significant benefits as an aerosol proxy when calculating ΔN_d and the radiative forcing from aerosol-cloud interactions. The large increase in predictive ability of ΔN_d when moving from AOD to AI for characterising the aerosol shows the importance of a measure of aerosol size, especially given the strong changes in aerosol type between the PI and the PD simulations. While

there is also a clear benefit from including vertical information (CCN_{1km} is a better proxy than colCCN for most GCMs), this increase in the accuracy when diagnosing the radiative forcing is smaller than that when using AI compared to AOD. The change in predictive ability when moving from AI to column integrated CCN is the smallest change, suggesting that information on aerosol composition is the least important of the three factors (vertical location, size distribution and composition) that limit the ability of the AOD- N_d relationship to characterise the strength of aerosol-cloud interactions [24].

Conclusions

In this work, multiple aerosol-climate models have been used to investigate how a change in cloud droplet number concentration (N_d) can be predicted from present day aerosol-cloud relationships.

The use of joint histograms normalised by aerosol occurrence is demonstrated, accounting for non-linearities in the aerosol- N_d relationship. It also removes the influence of the aerosol environment on the strength of the aerosol- N_d relationship, such that the present day and pre-industrial aerosol- N_d relationships are nearly identical with the correct choice of aerosol proxy (Fig. 1).

Although diagnosing the true sensitivity of N_d to cloud condensation nuclei (CCN) remains a difficult problem using only present day relationships [18], determining ΔN_d is much easier as it weights the calculation towards regions with a larger change in CCN, where the relationship can be determined with greater accuracy in (Fig. 2). If the change in CCN at 1km altitude (CCN_{1km}) between the pre-industrial (PI) and the present day (PD) is known, then the PD relationship between CCN_{1km} and the N_d is enough to diagnose the PD-PI change in N_d (ΔN_d) to within 20% of the value determined by the climate simulations (Fig. 3). Using joint histograms to account for non-linearities in the CCN- N_d relationship, a single global relationship between CCN_{1km} and N_d can be used, with only a small reduction in the accuracy of diagnosing ΔN_d and the instantaneous radiative forcing due to changes in cloud albedo (RFaci).

While vertical information is shown to be important in predicting ΔN_d , these results imply that information about the aerosol size distribution makes a dominant contribution to the accuracy of the predictions of ΔN_d , with the aerosol index (AI) showing significant gains over the aerosol optical depth (AOD), similar to previous work [15]. The estimates of the anthropogenic change in AI provided by the models in this work combined with AI- N_d joint histograms from satellite data provide a revised RFac estimate of around -0.4 Wm^{-2} , although there is a large diversity between the model estimates, ranging from -0.18 to -1.01 Wm^{-2} . The larger ΔN_d suggested by this work also suggests a larger ERFaci than previous studies [11], but this not investigated here. As estimates of the PD-PI aerosol environment are often generated from models, estimates of the PD-PI AI change could be calculated alongside AOD changes. Using AI has the advantage over using CCN since it is currently retrieved by satellite instruments (although retrieving CCN may be possible in certain situations [25]). This suggests that the AI is potentially a useful parameter to use when calculating observational constraints on the strength of RFac in liquid clouds and where possible should be considered for future observation-based investigations.

559
560
561
562
563
564
565
566
567
568
569
570
571
572
573
574
575
576
577
578
579
580
581
582
583
584
585
586
587
588
589
590
591
592
593
594
595
596
597
598
599
600
601
602
603
604
605
606
607
608
609
610
611
612
613
614
615
616
617
618
619
620

Materials and Methods

Throughout this work, output from several global aerosol-climate simulations performed as part of the AeroCom model inter-comparison project [18, 19] is used to provide simulations of the PD and PI atmospheres. Both PD and PI simulations are nudged to the same horizontal winds (2006-2010) and include PD greenhouse gases, sea surface temperatures and natural forcings. All of the models include interactive aerosol modules, that interact with the cloud via a modification of N_d , ice crystal number concentration and radiative fluxes. This affects the radiation as well as the precipitation formation in liquid clouds via autoconversion, leading to more complex effects on the cloud properties. The model data is regridded to a 2.5° by 2.5° resolution and averaged to daily temporal resolution. As this analysis focuses on liquid water clouds, only gridboxes with an ice water path of less than 5 g m^{-2} are used. Six of the nine available simulations were selected to provide a wide selection of models and microphysics schemes. The models themselves are self-consistent, such that an imperfect modelling of the aerosol or the cloud properties does not affect the conclusions.

ΔN_d is diagnosed for each 2.5° by 2.5° gridbox using the PD relationship between the aerosol parameter (A) and the N_d and the known change in the aerosol parameter between the PD and PI simulations. Eq. 1 shows how ΔN_d is diagnosed within each gridbox using a joint probability histogram between the aerosol and N_d created from PD relationships and the probability histograms of the PI and PD aerosol parameter in each gridbox.

$$\Delta N_d = \sum_{N_d} N_d \sum_A P(N_d|A)_{PD} \times (P(A)_{PD} - P(A)_{PI}) \quad [1]$$

If the OLS method is used, the calculation for ΔN_d is conceptually similar, using the ACI metric ($\frac{dN_d}{d \ln(A)}_{PD}$) from [5].

$$\Delta N_d = ACI_A \times (\overline{\ln(A_{PD})} - \overline{\ln(A_{PI})}) \quad [2]$$

where the overbar denotes an average over a distribution. To investigate the impact that errors in diagnosing ΔN_d have on the RFacI, the Twomey formula [26] is used to calculate the change in cloud albedo ($\alpha_{cl,d}$). The cloud albedo is calculated from the CERES TOA SW all-sky albedo and the MODIS Aqua L3 (MYD08_D3) collection 6 cloud optical properties cloud fraction [27], using only gridboxes with zero ice cloud. This is combined with the MODIS annual mean liquid cloud fraction (f_{liq}) and the downwelling solar flux (F^\downarrow) to produce a simple estimate of the RFacI (ΔF^\uparrow) [28].

$$\Delta F^\uparrow = -F^\downarrow f_{liq} \frac{\alpha_{cl,d}(1 - \alpha_{cl,d})}{3N_d} \Delta N_d \quad [3]$$

The MODIS AI is used to provide an observational constraint on the RFacI by generating AI- N_d joint histograms from observations. For these histograms, the N_d is calculated using the adiabatic approximation, as specified in [11]. The AI is calculated from the AOD-Angström exponent joint histogram in the MODIS MYD08_D3 product using only gridboxes where no ice cloud is detected (to reduce possible cirrus contamination). As the relative error of the MODIS AOD and hence the Angström exponent and AI is large at low AOD (<0.03), the N_d is assumed constant at AI values below 0.03.

ACKNOWLEDGMENTS. The model data was provided through the AeroCom initiative. The MODIS data was provided by the NASA Goddard Space Flight Center and the CERES data from the NASA Langley Research Center. This work received funding from the European Research Council under the European Union's Seventh Framework Programme (FP7/2007-2013) / ERC grant agreements no. FP7-306284 ("QUAERERE"), FP7-280025 ("ACCLAIM") and FP7-603445 ("BACCHUS"), the United Kingdom Natural Environment Research Council Grant NE/I020148/1, the Austrian Science Fund (J 3402-N29, Erwin Schrödinger Fellowship Abroad), the Environment Research and Technology Development Fund (S-12-3) of the Ministry of the Environment, Japan and JSPS KAKENHI Grant Number JP15H01728 and JP15K12190, the National Natural Science Foundation of China (grant no. 41575073 and 41621005), the Swiss National Supercomputing Centre (project s431) and the supercomputer system of the National Institute for Environmental Studies, Japan. The Pacific Northwest National Laboratory (PNNL) is operated for the Department of Energy (DOE) by Battelle Memorial Institute under Contract DE-AC06-76RLO 1830. Work at PNNL was supported by the US DOE Decadal and Regional Climate Prediction using Earth System Models program and by the US DOE Earth System Modeling program. The ECHAM6-HAM model was developed by a consortium composed of ETH Zurich, Max Planck Institut für Meteorologie, Forschungszentrum Jülich, University of Oxford, the Finnish Meteorological Institute, and the Leibniz Institute for Tropospheric Research, and is managed by the Center for Climate Systems Modeling (C2SM) at ETH Zurich which also provided technical and scientific support. The authors would like to thank Helen Brindley (Imperial College London) for her comments on the manuscript.

- Boucher O et al. (2013) *Clouds and Aerosols*, eds. Stocker T et al. (Cambridge University Press, Cambridge, United Kingdom and New York, NY, USA), p. 571–658.
- Twomey S (1974) Pollution and the planetary albedo. *Atm. Env.* 8:1251–1256.
- Albrecht B (1989) Aerosols, cloud microphysics, and fractional cloudiness. *Science* 245:1227–1230.
- Nakajima T, Higurashi A, Kawamoto K, Penner J (2001) A possible correlation between satellite-derived cloud and aerosol microphysical parameters. *Geophys. Res. Lett.* 28:1171–1174.
- Feingold G, Eberhard W, Veron D, M P (2003) First measurements of the Twomey indirect effect using ground-based remote sensors. *Geophys. Res. Lett.* 30:1287.
- Koren I, Kaufman Y, Rosenfeld D, Remer L, Rudich Y (2005) Aerosol invigoration and restructuring of Atlantic convective clouds. *Geophys. Res. Lett.* 32:L14828.
- Quaas J, Boucher O, Bellouin N, Kinne S (2008) Satellite-based estimate of the direct and indirect aerosol climate forcing. *J. Geophys. Res.* 113:D05204.
- Quaas J, Stevens B, Stier P, Lohmann U (2010) Interpreting the cloud cover - aerosol optical depth relationship found in satellite data using a general circulation model. *Atmos. Chem. Phys.* 10:6129–6135.
- Grandey BS, Gururaj A, Stier P, Wagner TM (2014) Rainfall-aerosol relationships explained by wet scavenging and humidity. *Geophys. Res. Lett.* 41:5678–5684.
- Jones TA, Christopher SA, Quaas J (2009) A six year satellite-based assessment of the regional variations in aerosol indirect effects. *Atmos. Chem. Phys.* 9:4091–4114.
- Gryspeerd E, Quaas J, Bellouin N (2016) Constraining the aerosol influence on cloud fraction. *J. Geophys. Res.* 121(7):3566–3583.
- Quaas J et al. (2009) Aerosol indirect effects - general circulation model intercomparison and evaluation with satellite data. *Atmos. Chem. Phys.* 9:8697–8717.
- Bellouin N et al. (2013) Impact of the modal aerosol scheme GLOMAP-mode on aerosol forcing in the Hadley Centre global environmental model. *Atmos. Chem. Phys.* 13:3027–3044.
- Shinozuka Y et al. (2015) The relationship between cloud condensation nuclei (CCN) concentration and light extinction of dried particles: indications of underlying aerosol processes and implications for satellite-based CCN estimates. *Atmos. Chem. Phys.* 15:7585–7604.
- Stier P (2016) Limitations of passive remote sensing to constrain global cloud condensation nuclei. *Atmos. Chem. Phys.* 16(10):6595–6607.
- Kaufman YJ et al. (2005) Aerosol anthropogenic component estimated from satellite data. *Geophys. Res. Lett.* 32:L17804.
- Penner JE, Xu L, Wang M (2011) Satellite methods underestimate indirect climate forcing by aerosols. *Proc. Natl. Acad. Sci. USA* 108:13404.
- Ghan S et al. (2016) Challenges in constraining anthropogenic aerosol effects on cloud radiative forcing using present-day spatiotemporal variability. *Proc. Nat. Acad. Sci.* 113:5804–5811.
- Zhang S et al. (2016) On the characteristics of aerosol indirect effect based on dynamic regimes in global climate models. *Atmos. Chem. Phys.* 16(5):2765–2783.
- Nam C, Bony S, Dufresne JL, Chepfer H (2012) The 'too few, too bright' tropical low-cloud problem in CMIP5 models. *Geophys. Res. Lett.* 39(21):L21801.
- Lebsock M, Stephens G, Kummerow C (2008) Multisensor satellite observations of aerosol effects on warm clouds. *J. Geophys. Res.* 113:D15205.
- Levy R et al. (2010) Global evaluation of the collection 5 MODIS dark-target aerosol products over land. *Atmos. Chem. Phys.* 10:10399–10420.
- Zelinka MD, Andrews T, Forster PM, Taylor KE (2014) Quantifying components of aerosol-cloud-radiation interactions in climate models. *J. Geophys. Res.* 119:7599–7615.
- Dusek U et al. (2006) Size matters more than chemistry for cloud-nucleating ability of aerosol particles. *Science* 312:1375–1378.
- Rosenfeld D et al. (2016) Satellite retrieval of cloud condensation nuclei concentrations by using clouds as ccn chambers. *Proc. Nat. Acad. Sci.* 113(21):5828–5834.
- Twomey S (1991) Aerosols, clouds and radiation. *Atm. Env* 25:2435–2442.
- Platnick S et al. (2003) The MODIS cloud products: algorithms and examples from Terra. *IEEE T. GeoSci. Remote* 41:459.
- Charlson RJ et al. (1992) Climate forcing by anthropogenic aerosols. *Science* 255:423–430.